Inorganic Chemistry

ARTICLE

pubs.acs.org/IC

In Situ X-ray Diffraction Study of Cesium Exchange in Synthetic Umbite

Christopher S. Fewox and Abraham Clearfield

Department of Chemistry, Texas A & M University, P.O. Box 30012, College Station, Texas 77842-3012, United States

Aaron J. Celestian*

Department of Geography and Geology, Advanced Materials Institute, Western Kentucky University, Bowling Green, Kentucky 42101-1066, United States

Supporting Information

ABSTRACT: The exchange of Cs^+ into $H_{1.22}K_{0.84}ZrSi_3O_9 \cdot 2.16H_2O$ (umbite-(HK)) was followed in situ using time-resolved X-ray diffraction at the National Synchrotron Light Source. The umbite framework (space group $P2_1/c$ with cell dimensions of a = 7.2814(3) Å, b = 10.4201(4) Å, c = 13.4529(7) Å, and β = 90.53(1)°) consists of wollastonite-like silicate chains linked by isolated zirconia octahedra. Within umbite-(HK) there are two unique ion exchange sites in the tunnels running parallel to the a-axis. Exchange Site 1 is marked by 8 member-ring (MR) windows in the bc-plane and contains K^+ cations. Exchange Site 2 is marked by a larger 8-MR channel parallel to [100], and contains H_2O molecules. The occupancy of the Cs^+ cations through these channels was modeled by Rietveld structure refinements of the diffraction data and demonstrated that there is a two-step exchange process. The incoming Cs^+ ions populated the larger 8-MR channel (Exchange Site 2) first and then migrated into the smaller 8-MR channel. During the exchange process a structural change occurs, transforming the exchanger from monoclinic $P2_1/c$ to orthorhombic $P2_12_12_1$. This structural change occurs when Cs^+ occupancy in the small cavity becomes greater than 0.50. The final in situ ion exchange diffraction pattern was refined to yield umbite-(CsK) with the molecular formula $H_{0.18}K_{0.45}Cs_{1.37}ZrSi_3O_9 \cdot 0.98H_2O$ and possessing an orthorhombic unit cell with dimensions a = 10.6668(8) Å, b = 13.5821(11) Å, c = 7.3946(6) Å. Solid state ^{133}Cs MAS NMR showed there is only a slight difference between the two cavities electronically. Valence bond sums for the completely occupied Exchange Site 1 demonstrate that Cs−O bonds of up to 3.8 Å contribute to the coordination of the Cs^+ cation.

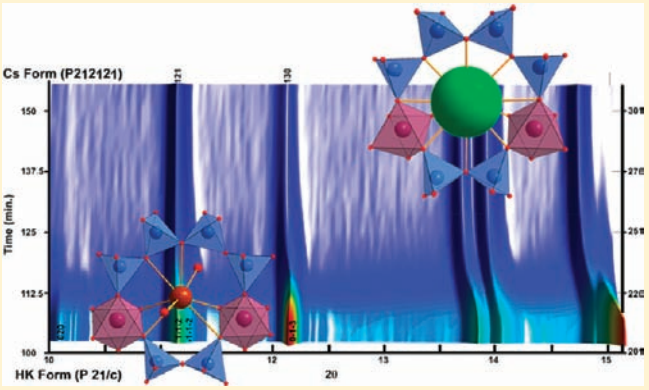

INTRODUCTION

Open framework inorganic compounds have a wide variety of uses including catalysis, gas separation, and ion exchange.[1−3] As ion exchangers they have shown to be robust at both ends of the pH scale and stable to high temperatures, oxidizing environments, and ionizing radiation. Because of their high ion selectivity and structural stability, inorganic ion exchangers have become increasingly important in the medical industry as radionuclide generators, and are currently being tested for use in nuclear waste remediation.[4−6] Many of these materials have tunable properties, such as the ability to alter pore size and enhance selectivity by making framework substitutions.[7−9] Determining the ion exchange mechanism and the physicochemical nature for the selectivity of these compounds may make it possible to tailor these compounds to suit specific engineering applications.

For decades, knowledge about the mechanism of ion exchange and intercalation has been derived from kinetic measurements coupled with studies of thermodynamic equilibrium quantities such as entropy, enthalpy, and energy of activation. To arrive at these quantities, certain principles about ion exchange have been granted an a priori understanding since the early 1900s, most notably, that the rate-determining step of an exchange process is a diffusion limited process; therefore it may be erroneous to think of it as an actual chemical exchange.[10] Other meaningful mechanistic information, such as diffusion coefficients, can be derived from time-resolved uptake data by fitting uptake curves to a variety of models given by Boyd et al. and others.[11,12] Application of the Nernst−Planck equations can permit formal definition of rate expressions; however, Helfferich warns against the physical interpretation of these values in the same manner as actual chemical reactions.[10]

Received: December 22, 2010
Published: March 04, 2011

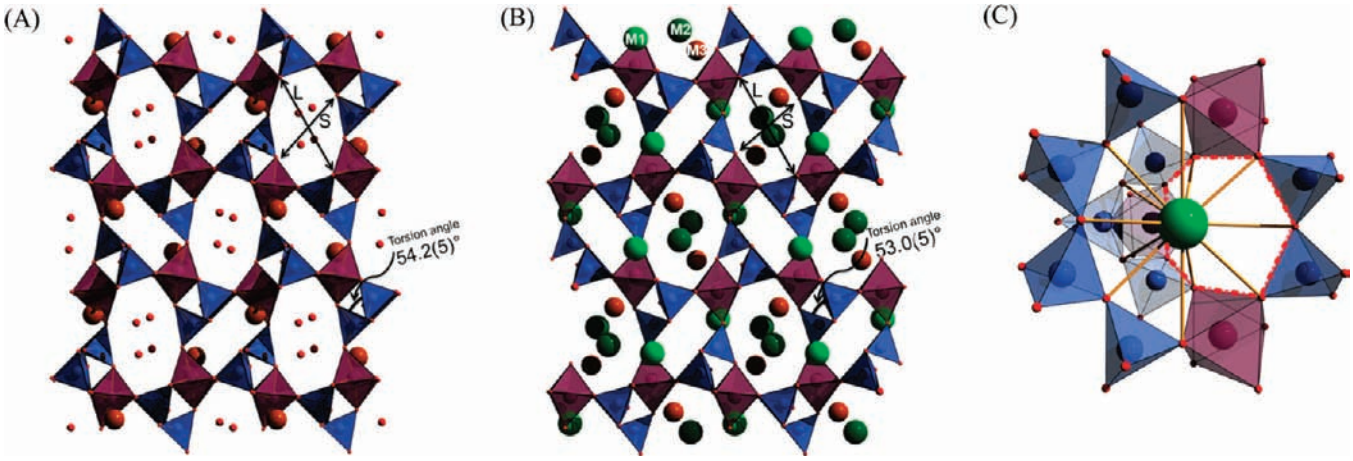

Figure 1. Structural overview of the "dry" umbite parallel to [100] in the monoclinic space group (A) and the Cs exchanged umbite structure (B) showing the larger Exchange Site 2 elliptical 8MR. Exchange Site 2 is centered at cation site M1. Torsion angle of the wollastonite chains is also illustrated. A perspective view approximately down the $[1\bar{1}0]$ showing the local bonding coordination around Cs to framework O^{2-} at Exchange Site 1 in the 8MR (C). The red dashed line outlines the 7MR in (C). Si−O tetrahedral blue, Zr−O octahedral purple, O red, interstitial H_2O shown as large red spheres, and K are orange spheres (H_2O and K sites not shown in (C) for clarity). Cation sites M1, M2, and M3 are labeled as integers at the top of (B). S:L ratio does not change significantly between umbite-(HK) (0.91) and Umbite-(CsK) (0.88). In (A), nonbonded O atoms (red) in the 8MR have been modeled at H_2O molecules, and their H-bonding scheme has not been depicted.

While the theory and experimental observations previously mentioned provide insight into the mechanism of ion exchange, they do not describe the paths of the cations through extended framework structures. Coupling the information given by theory and kinetic observations with structural data may provide the information needed to describe the atom site-by-site ion exchange mechanisms. Monitoring the exchange process in situ using X-ray diffraction (XRD) provides numerous advantages to ex situ ion exchange studies. Structural change in the framework can be monitored as the host and guest ions exchange, as well as being able to model the diffusion paths of ions to the exchange sites. Work of this nature has already been performed on inorganic framework materials with zeolite type pores.[13−16] Celestian and co-workers were able to describe the Na/K exchange behavior of the germanium analogue of the mineral gismondine and the Cs/H behavior in sitinakite using data gathered from in situ ion exchange time-resolved XRD studies.[13,14,17] O'Hare and co-workers have studied the intercalation and exchange mechanism of $[LiAl_2(OH)_6]Cl \cdot H_2O$ extensively by a variety methods including in situ XRD.[18−20]

A group of heterosilicates possessing the mineral umbite topology has been used as an exemplary system for inorganic ion exchangers with more complex channel networks.[21−29] Umbite has two unique ion exchange sites in the form of tunnels that are contained in the *ab*-plane (or the *bc*-plane in the H-exchange monoclinic phase). The first cation exchange site, denoted as Exchange Site 1, is the slightly puckered corrugated 8-MR (approximately 7 Å × 7.2 Å) tunnel consisting of six silica tetrahedra and two zirconia octahedra (Figure 1). These tunnels are connected in the *ab*-plane by another (6.1 Å × 7.8 Å) 8-MR channel, denoted as Exchange Site 2 (Figure 1), which is composed of four silica tetrahedra and four zirconia octahedra. Cations with small ionic radii (i.r. < K or ∼1.5 Å) such as Na, Li, or H are able to exchange through the corrugated tunnels within the *ab*-plane (Exchange Site 1), and larger cations are restricted because of the puckered nature of the zirconia octahedra (Figure 1). While ion exchange has been described with ex situ XRD methods supplemented with kinetic data,[30] the exchange mechanism through the framework and cation site occupancies are better described by time-resolved in situ XRD studies. It is the goal of this study to determine the site-by-site ion exchange mechanisms, and possible causes of structural transformations in this zirconium silicate with the umbite topology upon Cs^+ exchange.

EXPERIMENTAL SECTION

Synthesis of Starting Material Umbite-(K). The heterosilicate potassium zirconium trisilicate with the umbite topology, $K_2ZrSi_3O_9 \cdot H_2O$, was synthesized hydrothermally by modification of methods previously reported by Poojary et al.[29] Approximately 7.0 g of silicic acid (Aldrich) was dissolved in 45 mL of 4 M KOH (Aldrich) and 10 mL of isopropanol (Aldrich). Then 13.5 mL of a 70% solution of zirconium isopropoxide in isopropanol (Aldrich) was diluted with 10 mL of isopropanol and added dropwise to the previous solution. Isopropyl alcohol was added to suppress the formation of hydrous zirconia. The mixture was divided in half and placed in 100 mL Teflon lined autoclaves and heated at 180 °C. After 5 days a white precipitate was isolated, washed with distilled water, and dried at 60 °C.

Umbite-(HK). There are several advantages of using a H^+ exchanged material for ion exchange studies. First, the exchange process is often accelerated when the microporous material is in a H^+ exchanged form.[31] This ensures the best chances that the entire exchange process will be observed during a single experiment at the synchrotron facility. Second, H^+ does not contribute significantly to the powder XRD pattern. Therefore any change observed in the calculated Fourier difference maps may be attributed to the in-going cation and minimizes the confusion of intracrystalline cation migration. Third, the application of this material may require it to be emerged in a caustic solution, and having a H^+ exchange microporous framework will serve to decrease the pH of the overall solution.

Umbite-(HK) ($H_{1.22}K_{0.84}ZrSi_3O_9 \cdot 2.16H_2O$) was made by shaking umbite-(K) in 0.1 M acetic acid at a volume to mass ratio of 500:1 for 24 h. The product was collected by vacuum filtration and washed with distilled water and acetone. The dry product was then shaken in 0.5 M acetic acid for 24 h. The product was again collected by vacuum filtration and rinsed thoroughly with distilled water and acetone.

In Situ Ion Exchange Study. The apparatus used for the time-resolved ion exchange studies was previously detailed by Celestian and co-workers.[32] Time resolved studies were performed at the X7B beamline (λ = 0.9221(1) Å), National Synchrotron Light Source, Brookhaven National Laboratory. Diffraction data were collected on a MAR 345 imaging plate

dx.doi.org/10.1021/ic102546w |*Inorg. Chem.* 2011, 50, 3596–3604

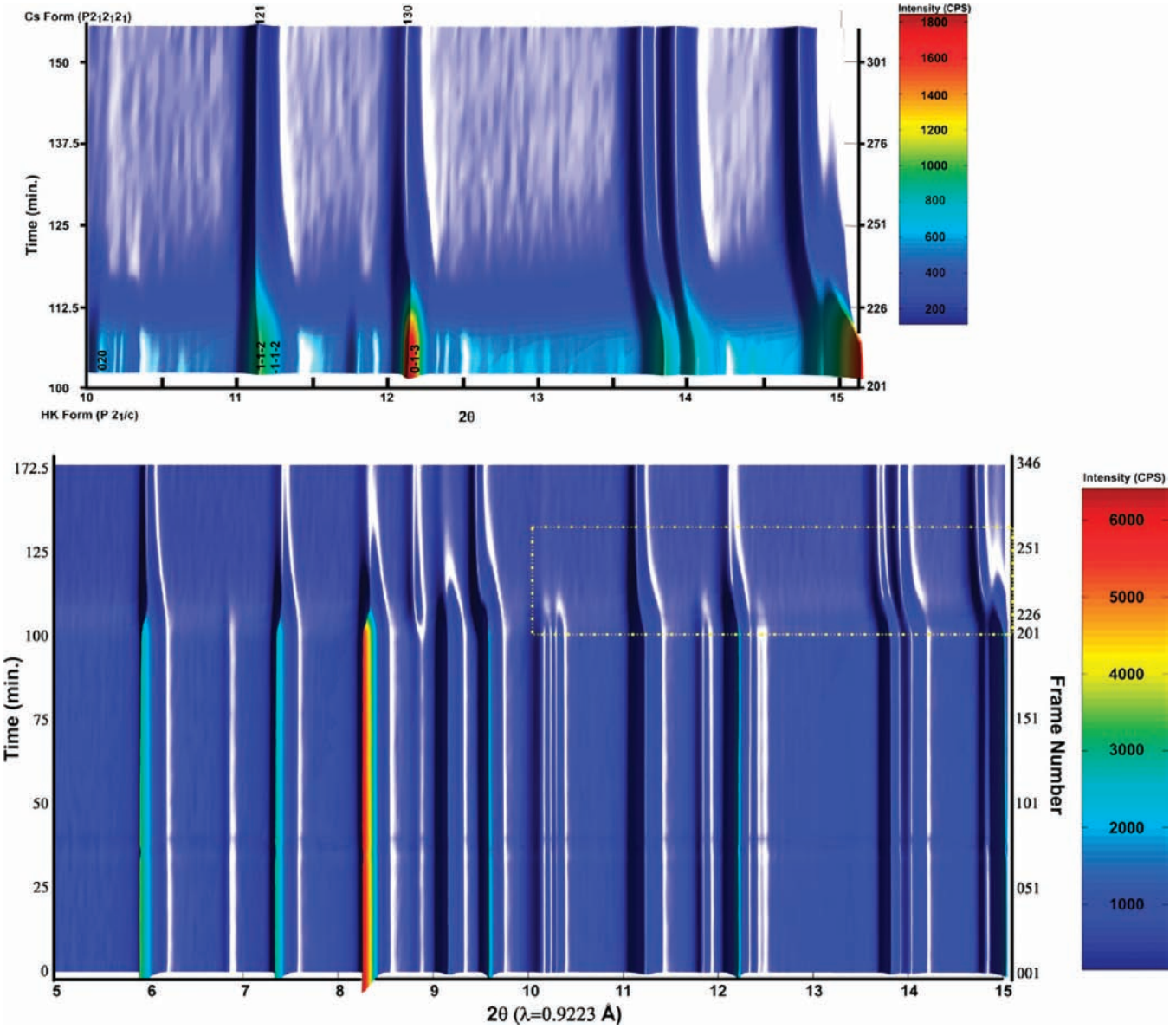

Figure 2. Time resolved XRD patterns for the ion exchange of Cs^+ into umbite-(HK) showing only data from 5°−15° 2θ (bottom). Yellow box outline is the inset area for (top). The onset of the structural transition is observed between frame 226 and 231 (times 112.5 min and 115 min). Cs occupancy values as determined by Rietveld structure refinements for each frame from 201 until the end of the experiment are presented in Table 5.

detector. Data collection time was 60 s. The goniometer was rotated 1° per second with respect to φ with a fixed χ of 90°. Imaging of the plate detector and dumping of the data lasted 80 s bringing the total time resolution to 140 s. Diffractometer constants such as beam center, detector pitch, yaw, and distance were calibrated from a LaB_6 standard.

Approximately 0.01 g of umbite-(HK) was ground and loaded into the capillary. A dry frame of umbite-(HK) was captured and then a wet frame with only deionized water flowing through the capillary was captured. The initial ion exchange solution was prepared by adding 0.011 g of CsCl to 200 mL of deionized water (approximately 0.32 mM CsCl). This solution was allowed to flow over the sample at constant 1 mL/minute for 40 frames (100 min.). After the first 40 frames (100 min.), the first three most intense peaks had a $\Delta 2\theta_{max}$ = 0.003°. To accelerate the exchange process, an additional 0.1 g of CsCl was added bringing the total concentration of Cs^+ to 3.3 mM with a constant flow rate of 1 mL/minute. Data were collected consecutively for approximately 1 h (Figure 2). After collecting the time-resolved data, the peristaltic pump was turned off, the exposure time was increased to 10 min, and φ was rotated thru 60° at 0.1° per second to collect a final frame on the wetted sample in an effort to achieve the best signal-to-noise ratio of the final exchanged material.

Data from the image-plate were integrated using the Fit2D software package[33−36] and the resulting 1D powder diffraction patterns were indexed using TREOR, ITO, and DICVOL methods found in the Fullprof program suite.[37] Full pattern profile fitting using the Le Bail method and Rietveld refinement were accomplished using the GSAS and EXPGUI program suite.[38−41]

Structure refinements from the powder data were initiated by using the framework atomic coordinates found for the umbite-(HK) structure as a starting model.[42] Later, for the orthorhombic phases beginning at frame 231 (115 min.) and beyond, the framework atomic parameters derived from the pure umbite-(K) structure were used as a starting model.[29] Bond distance constraints were applied for Si−O and Zr−O and set to 1.60 Å−1.68 Å, and 1.97 Å−2.2 Å, respectively. Isotropic atomic displacement parameters for all atoms were not refined, but fixed to previously reported values.[42] Once least-squares refinement

Table 1. Unit Cell and Refinement Statistics for the Starting and Ending Materials

	Umbite-(HK)[a]	Umbite-(CsK)[b]
formula weight$_{calc}$	389.05	536.17
space group	$P2_1/c$	$P2_12_12_1$
a (Å)	7.2814(3)	7.3946(6)
b (Å)	10.4201(4)	10.6668(8)
c (Å)	13.4529(7)	13.5821(11)
β	90.53(1)°	
V (Å^3)	1020.67(8)	1071.31(15)
Z	2	4
D_{calc} (g/cm^3)	2.517	3.318
no. of reflections	238	174
R_{wp} [b]	0.0377	0.0204
R_p [b]	0.0280	0.0144

[a] $H_{1.22}K_{0.84}ZrSi_3O_9 \cdot 2.16H_2O$; [b] $H_{0.18}K_{0.45}Cs_{1.37}ZrSi_3O_9 \cdot 0.98H_2O$. [b] Best R_{wp}, R_p = 0.0166, 0.0122 at frame 346 (time = 172.5 min) and worst R_{wp}, R_p = 0.0578, 0.0429 at frame 226 (time = 112.5 min).

Table 2. Selected Framework Bond Distances (Å)

bond	Umbite-(HK)	Umbite-(CsK)
Zr1—O5	2.161(13)	2.118(7)
Zr1—O6	2.067(16)	1.976(10)
Zr1—O7	1.982(13)	2.075(8)
Zr1—O8	1.978(16)	2.024(11)
Zr1—O9	1.986(17)	2.035(10)
Zr1—O10	2.015(17)	2.067(10)
Si2—O6	1.676(15)	1.644(9)
Si2—O9	1.652(19)	1.659(11)
Si2—O11	1.640(15)	1.651(9)
Si2—O13	1.655(17)	1.649(10)
Si3—O5	1.667(16)	1.646(9)
Si3—O7	1.626(17)	1.663(15)
Si3—O12	1.659(17)	1.662(10)
Si3—O13	1.665(17)	1.67(1)
Si4—O8	1.664(18)	1.658(11)
Si4—O10	1.661(15)	1.635(9)
Si4—O11	1.625(15)	1.638(8)
Si4—O12	1.627(16)	1.65(1)

converged to a $\chi^2 < 8$ (arbitrary value set by authors), Fourier difference maps were calculated, and searched for electron densities corresponding to positions of the charge balancing cations and extra-framework O (interpreted as H_2O). Since no analytical data were available for the Cs exchanged end-member, starting occupancies for H_2O, K, and Cs were estimated. Fourier difference maps were again calculated, and the site occupancies were adjusted until the value of ρ was less than 2 e$^-$ per Å^2, and any residual electron density did not make chemical sense (e.g., short bond distances, overlapping atom positions). Extra-framework cation positions were then refined while holding framework positions fixed. Once the positions of the extra-framework cations stabilized the framework atoms were refined while holding the cation positions fixed. This iterative approach was continued until all atom positions could be refined together, and the shift in atomic position was less than ±0.001 Å.

To model the disorder, Cs, K, and O (H_2O) atoms were placed at each extra framework site, and their atomic coordinates were constrained such that any refinement of position moved each atom to the same point in space. A similar method was used by Poojary and co-workers to model the disorder encountered while solving the ion exchange structures of the potassium phase.[29] Sites M1, M2, and M3 correspond to cations in Exchange Site 1 within the corrugated channel, cations in Exchange Site 2, and the H_2O site in Exchange Site 2, respectively (Figure 1). The sum of individual occupancies was constrained to unity, and initial occupancy values were set to 1/3 for each atom in sites M1, M2, and M3. No attempt to describe the positions of the H on the H_2O was made. This method likely underestimates the total amount O (H_2O) in the extra-framework sites, and future studies will be conducted to constrain the total amount of H_2O in the framework coupled with neutron diffraction studies to determine the H/D positions.

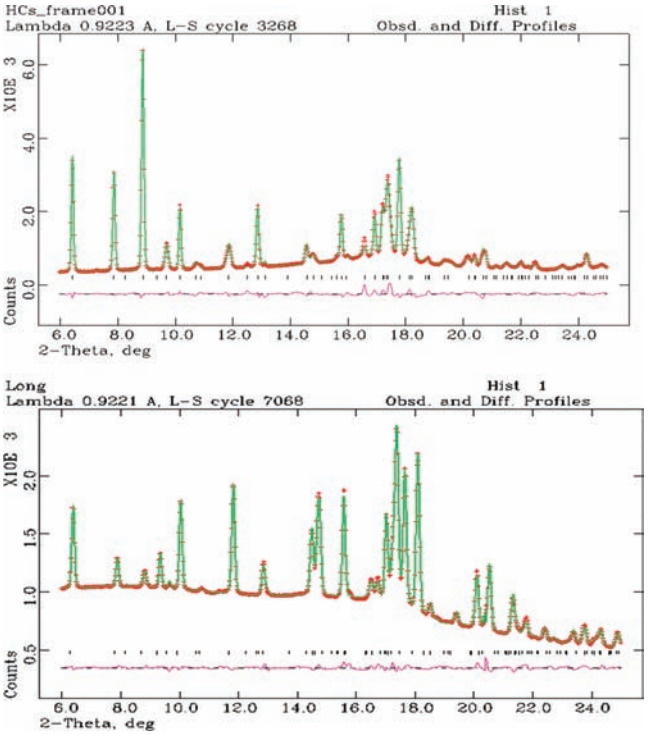

Figure 3. Example results of the Rietveld refinement and their difference plots for umbite-(HK) (top) and umbite-(CsK) (bottom). Raw data (red), calculated profile (green), difference curve (magenta), peak marker (black).

Nuclear Magnetic Resonance. Nuclear magnetic resonance can provide a secondary verification of the local coordination environment around the exchanged cation to corroborate the models derived Rietveld structure refinements. An analysis of the Bragg peaks in XRD patterns provides long-range structural information, and short-range local disorder of cations is sometimes difficult to accurately model based on diffraction data alone. The use of NMR provided verification of the various disordered Cs site positions in the channels of the umbite structure. ^{133}Cs MAS NMR experiments were performed on a Bruker Avance-400 equipped with standard 4 and 7 mm MAS and wide line probe heads. An external standard of solid CsCl dried at 60 °C for 3 days was used. Two samples of umbite-(HK) were loaded to a Cs^+ content of 5% and 75%.

RESULTS

Structure of $H_{1.22}K_{0.84}ZrSi_3O_9 \cdot 2H_2O$ Umbite-(HK). Unit cell parameters and refinement statistics are found in Table 1. Selected bond distances for the framework atoms in compounds umbite-(HK) and are listed in Table 2. The final refinement difference plot for compounds umbite-(HK) and are shown in Figure 3. The structure of umbite-(HK) was derived from

dx.doi.org/10.1021/ic102546w |Inorg. Chem. 2011, 50, 3596–3604

Rietveld refinement of the first "wet" frame 001 (0 min.). The structure of the partially protonated phase has been discussed in previous work.[42] The framework consists of wollastonite-like chains of silicate tetrahedra, and these chains are corner-shared by isolated zirconia octahedra. Identical to the channel network in the umbite-(K) parent compound, this arrangement gives rise to two unique channels and ion exchange sites which run perpendicular to each other and contain the extra-framework cations and interstitial H_2O. Exchange Site 1 is a corrugated 8-MR containing two cations that does not form a continuous channel for larger cations (e.g., ionic radius > K^+), and is composed of two Zr−O octahedra and six Si−O tetrahedra. Exchange Site 2 is a larger 8-MR (composed of four Zr−O octahedra and four Si−O tetrahedra) initially containing two extra-framework cations and two H_2O molecules.

The major differences between the as synthesized umbite-(K) and protonated umbite-(HK) are the positions of the extra-framework cations and H_2O and the space group. Umbite-(HK) forms with the monoclinic space group $P2_1/c$ with unit cell dimensions of a = 7.2814(3) Å, b = 10.4201(4) Å, c = 13.4529(7) Å, and β = 90.53(1)°. The parent compound, umbite-(K), crystallizes in an orthorhombic space group of $P2_12_12_1$, and has cell dimensions of a = 10.2977(2) Å, b = 13.3207(3) Å, c = 7.1956(1) Å.[29] After conversion to the protonated phase, all of the K^+ cations are located in Exchange Site 1 and are no longer dispersed over both exchange sites. The cation positions in Exchange Site 2 are now occupied entirely by H_2O molecules. This arrangement of the K^+ cations represents the "dry" sample described by Clearfield and Fewox in previous work[42] and is the starting material for the ion exchange studies in this work. The use of the term "dry" is differentiated from the "wet" sample because upon being immersed in flowing water, some of the K^+ spontaneously migrate out of Exchange Site 1, and move into Exchange Site 2. After wetting the umbite-(HK) sample in a flow-through cell, the majority of K^+ ions remained in Exchange Site 1 with an occupancy factor of approximately 0.64 for M1, while the remainder of the K^+ cations were found in Exchange Site 2 with occupancy factor of approximately 0.2 at site M2. The "dry" umbite has K^+ only in Exchange Site 1, while the "wet" umbite has K^+ in both Exchange Site 1 and Exchange Site 2. The cause of K^+ migration induced by flowing water over, and through the sample, is unknown. However, upon drying, the K^+ positions revert back to being fully occupied in Exchange Site 1. This process was only observed in the umbite-(HK) phase, as there were no measurable differences between atomic positions and occupancies of the "dry" and "wet" structures after Cs ion exchange.

Time-Resolved Exchange of Cs^+ in Umbite-(HK). Time resolved in situ XRD patterns are shown in Figure 2, and 69 frames were collected over a time period of approximately 172.5 min. Frames were automatically numbered beginning with 1 and increasing in steps of 5 such that the next frame after 001 would be named 006. This is the naming scheme imposed by the MAR345 image acquisition software.

During the first 40 min of ion exchange using the low concentration solution (approximately 0.32 mL CsCl), the first three most intense peaks (2θ = 6.06°, 7.43°, and 8.36°) decreased by less than ≈0.003° 2θ max. All diffraction patterns were indexed, and their unit cell dimensions refined. Within the first 40 min, the unit cell volume decreased by ≈0.01% (or $\Delta V \approx -3(1)$ Å^3). Fourier difference maps were calculated and searched for unaccounted electron density; however, no electron densities were found greater than 2 eV per Å^2 in crystallographic locations that would be chemically reasonable (i.e., acceptable bond lengths or angles). This indicated that only small changes had slowly occurred during the first 40 min of the ion exchange experiment, but we were unable to model whether Cs was entering the crystal structure or H_2O molecules were slowly removed using the Rietveld Method. For ion exchange to be observed within the allowed time frame of the experiment at the X7B beamline, the Cs concentration in the exchange solution was increased.

Table 3. Refined Unit Cell Dimensions for Diffraction Patterns 201−346

time (min)	frame	a (Å)	b (Å)	c (Å)	β (deg)	volume (Å^3)
172.5	346	10.695(3)	13.501(1)	7.3465(9)		1060.79
170	341	10.697(2)	13.498(1)	7.3453(8)		1060.72
167.5	336	10.696(3)	13.499(1)	7.3464(9)		1060.74
165	331	10.627(3)	13.504(1)	7.3465(8)		1054.35
162.5	326	10.621(3)	13.512(2)	7.3415(10)		1053.64
160	321	10.594(3)	13.497(1)	7.3442(9)		1050.22
157.7	316	10.634(2)	13.498(3)	7.3439(9)		1054.00
155	311	10.592(3)	13.504(3)	7.3447(8)		1050.65
152.5	306	10.619(2)	13.500(3)	7.3431(7)		1052.80
150	301	10.592(3)	13.501(3)	7.3449(9)		1050.36
147.5	296	10.592(3)	13.506(3)	7.3447(9)		1050.84
145	291	10.590(2)	13.504(2)	7.3438(9)		1050.27
142.5	286	10.591(2)	13.503(3)	7.3443(8)		1050.33
140	281	10.590(2)	13.508(2)	7.3437(8)		1050.62
137.5	276	10.588(3)	13.507(1)	7.3424(7)		1050.09
135	271	10.587(3)	13.508(1)	7.3427(10)		1050.15
130	261	10.587(2)	13.510(2)	7.3419(8)		1050.16
127.5	256	10.584(2)	13.506(1)	7.3398(9)		1049.31
125	251	10.585(3)	13.509(3)	7.3398(8)		1049.60
122.5	246	10.582(3)	13.505(2)	7.3391(9)		1048.85
120	241	10.579(2)	13.504(3)	7.3370(8)		1048.24
117.5	236	10.578(2)	13.505(2)	7.3364(8)		1048.09
115	231	10.574(3)	13.510(1)	7.3357(8)		1048.07
112.5	226	13.492(3)	10.566(3)	7.3248(8)	90.22(7)	1044.26
110	221	13.478(1)	10.560(2)	7.3195(7)	90.19(4)	1041.88
107.5	216	13.435(1)	10.439(3)	7.2881(8)	90.32(9)	1022.29
105	211	13.406(1)	10.436(3)	7.2756(8)	90.26(8)	1017.98
102.5	206	13.424(4)	10.430(6)	7.2814(11)	90.30(9)	1019.56
100	201	13.426(2)	10.426(3)	7.2789(9)	90.22(2)	1018.96

Frames 201 (100 min.) through 346 (172.5 min) (Figure 2), the concentration of the solution was increased from 0.32 mM to 3.3 mM. All diffraction patterns, including the final diffraction pattern collected over 10 min, were indexed and unit cell dimensions are listed in Table 3. The unit cell volume increases steadily from ≈1019 Å^3 in frame 201 (100 min.) to ≈1061 Å^3 in frame 346 (172.5 min). The transition from the monoclinic to the orthorhombic crystal system occurs within one diffraction pattern between frames 226 and 231 (112.5 to 115 min.) (Figure 4). From frame 201 (100 min.), there was a rapid uptake of Cs into Exchange Site 1 which continued filling at a constant rate until frame 226 (112.5 min.). After 12.5 min from the onset of measurable ion exchange, the structure transformed from space group $P2_1/c$ to $P2_12_12_1$. After the structural transformation and within the three following diffraction patterns (7.5 min.), Cs rapidly filled Exchange Site 1 to an occupancy of ≈0.65 and Cs rapidly filled Exchange Site 2 to an occupancy of ≈0.24

dx.doi.org/10.1021/ic102546w |Inorg. Chem. 2011, 50, 3596–3604

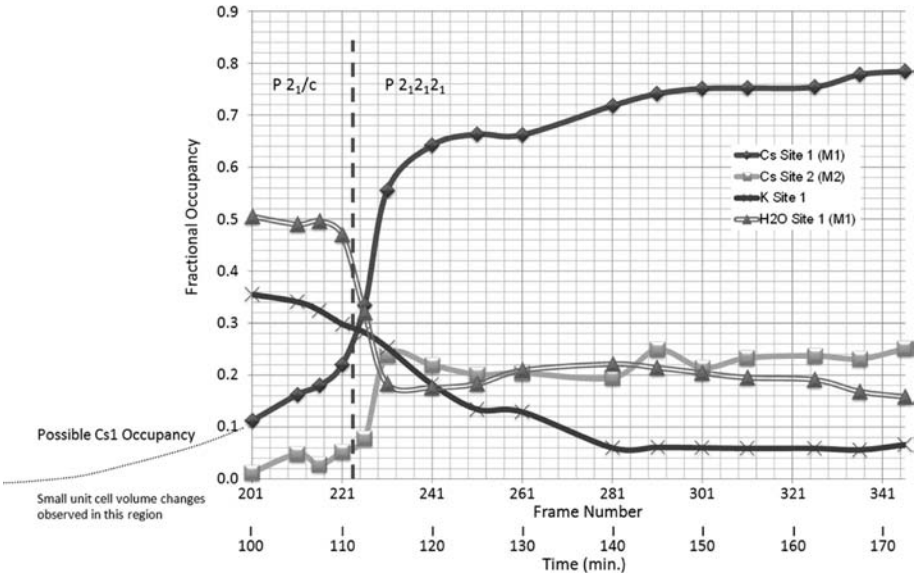

Figure 4. Plot of select Cs1, Cs2, and K1 fractional occupancies modeled using the Rietveld Method. Error bars are smaller than data points and data point connectors are for visual effect only. Possible Cs1 occupancy trend also shown prior to frame 201 as an unmeasured dashed line. The abrupt update of Cs at frame 231 (115 min.) may suggest rapid H^+ exchange out of the framework at the onset of the structural transition. Using site OW2 may be a good proxy to the amount of H^+ in the structure. That is, if H^+ were to be removed from the structure, then the $H\cdots OH_2$ hydrogen-bond network would be disrupted and therefore H_2O may be less likely to occupy space in the structure. Dehydration of the framework did occur during this ion exchange, but the precise mechanisms (and above discussion) cannot be verified without neutron diffraction data. Occupancy trend of Cs1 prior to frame 201 is based on evidence of minor unit cell volume changes; however, no evidence of electron density associated with Cs could be modeled at Exchange Site 1 between minutes 0−100 (frames 1−201). Vertical dashed line indicates event of space symmetry transformation.

(Figure 4). After the second surge of occupancy of Cs, the exchange rate slowed. A simplified schematic of the proposed ion exchange process is shown in Figure 5, and refined extra-framework occupancies are presented in Table 5.

Structure of $H_{0.18}K_{0.45}Cs_{1.37}ZrSi_3O_9\cdot 0.98H_2O$ Umbite-(CsK). Data for the final diffraction pattern were collected over a 10 min exposure. Rietveld refinement of models to these data showed that the unit cell had expanded to approximately 1071 $Å^3$. The structure of umbite-(CsK) transformed from the monoclinic $P2_1/c$ space group to the orthorhombic space group $P2_12_12_1$ with cell dimensions of a = 10.6668(8) Å, b = 13.5821(11) Å, c = 7.3946(6) Å. Exchange Site 1 is solely occupied by Cs^+ while the remainder of the K^+ cations are found in Exchange Site 2 disordered among sites M2 and M3 with occupancy factors 0.35 and 0.1, respectively. The H_2O molecules are found in the Exchange Site 2 with occupancies in M2 and M3 of 0.26 and 0.8, respectively. Cation-oxygen distances for M1−O, M2−O, and M3−O are shown in Table 4. Average Cs−O bond distance in Exchange Site 1 is 3.434(43) Å.

NMR. The ^{133}Cs MAS NMR of a 5% and 75% Cs^+ loaded sample of umbite-(CsK) is seen in Figure 6. At 5% Cs^+ occupancy the chemical shift from the CsCl standard was −165 ppm. In the 75% Cs^+ loaded sample the chemical shift was −172 ppm.

Valence Bond Sums. Valence bond calculations were performed using eq 1[43] and calculated in the program VaList.[44]

$$S_{ij} = \exp\left(\frac{R_o - R_{ij}}{b}\right) \quad (1)$$

Values of R_o and b are 2.417 and 0.370, respectively. Fourteen Cs−O contacts are reported with bond lengths shorter than 4.0 Å. Values of S_{ij} for these 14 Cs−O contacts in Exchange Site 1 are listed in Table 6. The valence bond sum, ΣS_{ij}, is 1.003, completely accounting for a charge of +1 on Exchange Site 1 Cs cations.

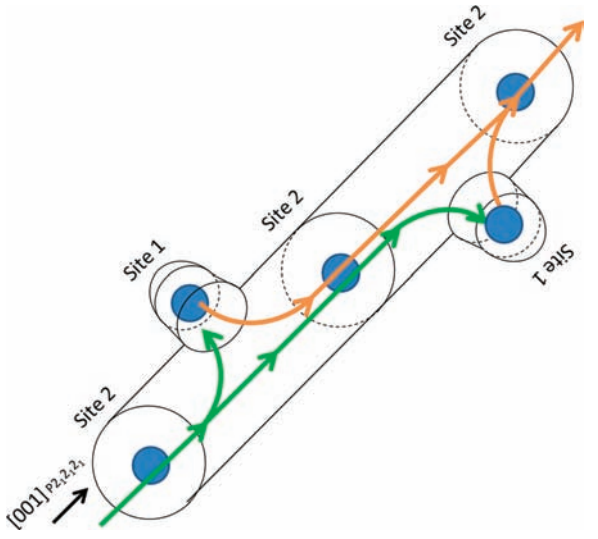

Figure 5. Simplified schematic of the overall two-step ion exchange diffusion process. First, Cs slowly exchanges into Site 1 displacing K at Exchange Site 1. Second, a symmetry change is induced by disorder within the [001] channel at frame 226. The amount of Cs occupancy in Exchange Site 1 required to induce the loss of symmetry is approximately 0.33 site occupancy. Third, Cs then quickly diffuses into the channels at Exchange Sites 1 and 2. Blue spheres represent K or Cs atom site locations, Cs exchange path shown in green, K exchange path shown in orange.

DISCUSSION

Rietveld refinements for selected frames from 201 (100 min) through 346 (172.5 min) model the changing occupancies of the cations as they migrate to and from the exchange sites. Cation site occupancies for refined models to the diffraction patterns are listed in

dx.doi.org/10.1021/ic102546w |Inorg. Chem. 2011, 50, 3596–3604

Table 4. Extra-Framework Cation-Oxygen Bond Distances[a]

compound	M1[b]—O	distance (Å)	M2[b]—O	distance (Å)	M3[b]—O	distance (Å)
Umbite -HK	M1—O6	2.967(27)	M2—O5	3.026(36)		
	M1—O8	3.420(25)	M2—O7	3.152(32)		
	M1—O9	3.135(25)	M2—O8	2.648(27)		
	M1—O10	2.757(27)	M2—O10	2.882(29)		
	M1—O11	3.669(19)	M2—O11	3.342(29)		
	M1—O12	3.454(20)	M2—Ow1	2.734(39)		
	M1—O13	3.454(20)				
	M1—Ow1	2.821(30)				
Umbite-CsK	M1—O6	3.407(41)	M2—O6	3.200(32)	M3—O5	3.653(34)
	M1—O7	3.789(57)	M2—O8	3.129(21)	M3—O5′	3.080(41)
	M1—O7′	3.657(57)	M2—O9	3.437(21)	M3—O7	3.348(46)
	M1—O8	3.405(35)	M2—O10	2.980(24)	M3—O8	3.112(30)
	M1—O9	3.240(34)	M2—O1	2.964(17)	M3—O10	3.512(28)
	M1—O10	3.211(36)	M2—Ow1	2.921(24)		
	M1—O11	3.845(22)	M2—Ow1′	2.731(30)		
	M1—O11′	3.320(23)				
	M1—O12	3.375(23)				
	M1—O12′	3.387(34)				
	M1—O13	3.499(25)				
	M1—O13′	3.265(33)				
	M1—Ow1	3.240(44)				
	M1—Ow3	3.878(14)				

[a] Apostrophes indicate symmetrically equivalent sites. [b] In umbite-(HK) M1 = K15, M2 = K14. In umbite-(CsK) M1 = Cs14, M2 = Cs16|K16, M3 = Cs15|K15.

Table 5. First, Cs^+ slowly exchanges into the puckered 8-MR channel (Exchange Site 1), which displaces K^+ into the uncorrugated 8-MR (Exchange Site 2). This initial Cs^+ diffusion process was slow (approximately 100 min.). Once the K^+ occupancy in Exchange Site 1 has been reduced to approximately 0.35, the rate of Cs^+ cation diffusion increases and occupies sites in Exchange Site 1 and Exchange Site 2. As exchange continues, K^+ is eventually completely displaced from the puckered 8-MR leaving only Cs^+. The occupancy level of K^+ in the large channel increases from 0.25 to 0.35 as K^+ diffuses in from the puckered 8-MR channel and eventually out to solution (Figure 5).

Changes in interstitial H_2O content also occur with increasing Cs^+ incorporation. The amount of H_2O in Exchange Site 1 decreases to zero occupancy (0.00(5)) as Cs^+ moves into the puckered 8-MR. It should be noted that there could be residual H_2O at site M1 which caused significant disorder at site M1; however, it could not be modeled using the current XRD data sets and during the refinements it was fixed to be 0. Work is currently underway to obtain more robust occupancy parameters for H_2O and Cs at site M1. The H_2O in the M3 cation position moves to the M2 position, and at the end of the exchange experiment, an entire mole of H_2O per mole of exchanger is returned to solution. Cation sites M2 and M3 in the large channel were finally populated by H_2O, K^+, and Cs^+.

An explanation for the structural transition from a monoclinic to an orthorhombic crystal system is evident from the comparison of the umbite structures. The main consequence of the transformation is the loss of the c-glide. If the special positions in the $P2_1/c$ space group are transformed to the $P2_12_12_1$, the inversion centers are found in Exchange Site 1, the smaller puckered 8-MR cavity. If the inversion center holds true, then a distance between any atom and the symmetrically equivalent atom should be equidistant if reflected through the center of symmetry. Indeed this holds true for the framework atoms in the $P2_12_12_1$ space group. Extra-framework cations and H_2O in Exchange Site 2 (M2, M3) do not have equivalent positions after applying the inversion operator and therefore the center of inversion is destroyed. The loss of the inversion occurs after K^+ occupancy in Exchange Site 1 is reduced to approximately 0.35. The positional disordering of the extra-framework cations and H_2O destroys the center of symmetry and the c-glide in the monoclinic structure and causes a shift to the noncentrosymmetric orthorhombic space group. There is no significant shift in framework bond angles or bond distances during the ion exchange process or symmetry transitions.

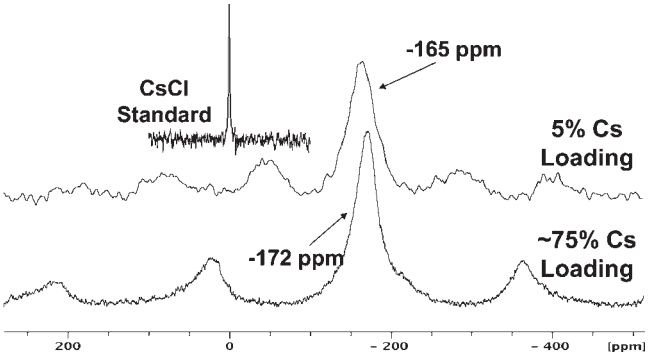

Figure 6. ^{133}Cs MAS NMR spectra for 5% Cs and 75% Cs site occupancy exchange. NMR spectra for the CsCl standard shown as inset.

Since Cs^+ cations demonstrate preference for occupancy in Exchange Site 1 over Exchange Site 2, it was suspected that the ^{133}Cs MAS NMR would show a difference in the electronic surroundings of these cations, displaying two distinct resonances as %Cs occupancy increased. At approximately 5% Cs occupancy,

dx.doi.org/10.1021/ic102546w |Inorg. Chem. 2011, 50, 3596–3604

Table 5. Refined Fractional Occupancies of Cs^+, K^+, and H_2O (O) for Selected Frames

time (min.)	frame	Cs Site 1 (M1)[a]	Cs Site 2 (M2)[a]	Cs Site 2 (M3)[a]	K Site 1 (M1)[a]	K Site 2 (M2)[a]	H_2O (M1)[a]	H_2O (M2)[a]	H_2O (M3)[a]
100	201	0.11(2)	0.01(2)	0.00(8)	0.35(5)	0.25(4)	0.50(5)	0.54(4)	0.99(2)
105	211	0.16(2)	0.04(8)	0.00(2)	0.34(1)	0.26(4)	0.49(1)	0.46(2)	0.99(1)
107.5	216	0.18(1)	0.02(8)	0.01(2)	0.32(4)	0.28(6)	0.49(6))	0.51(8)	0.92(4)
110	221	0.22(1)	0.05(2)	0.01(1)	0.29(8)	0.30(4)	0.47(0)	0.47(5)	0.88(3)
112.6	226	0.33(4)	0.07(8)	0.05(1)	0.28(2)	0.30(4)	0.32(1)	0.51(1)	0.90(4)
115	231	0.55(5)	0.23(8)	0.04(8)	0.25(3)	0.31(1)	0.18(3)	0.42(1)	0.90(2)
120	241	0.64(2)	0.21(9)	0.07(1)	0.18(2)	0.34(1)	0.17(6)	0.41(9)	0.86(9)
125	251	0.66(3)	0.20(1)	0.09(4)	0.13(4)	0.34(1)	0.18(3)	0.36(0)	0.84(2)
130	261	0.66(2)	0.20(4)	0.10(1)	0.12(9)	0.34(3)	0.20(9)	0.33(8)	0.83(0)
140	281	0.71(8)	0.19(5)	0.17(3)	0.06(1)	0.34(5)	0.22(1)	0.29(2)	0.75(7)
145	291	0.74(1)	0.24(9)	0.18(4)	0.06(1)	0.34(7)	0.21(4)	0.27(5)	0.75(1)
150	301	0.75(1)	0.21(4)	0.18(1)	0.06(1)	0.34(4)	0.20(4)	0.26(2)	0.74(4)
155	311	0.75(2)	0.23(3)	0.17(1)	0.05(9)	0.34(3)	0.19(5)	0.22(8)	0.74(7)
162.5	326	0.75(4)	0.23(7)	0.17(3)	0.05(9)	0.34(8)	0.19(1)	0.22(7)	0.71(9)
167.5	336	0.77(8)	0.23(1)	0.17(1)	0.05(6)	0.35(2)	0.16(8)	0.22(9)	0.71(2)
172.5	346	0.78(4)	0.25(1)	0.17(3)	0.06(6)	0.36(3)	0.15(8)	0.22(3)	0.72(1)
	long	1.00	0.23(0)	0.14(3)	0.00	0.35(3)	0.00	0.29(9)	0.76(1)

[a] See Figure 1 for the graphical representation of these sites in the umbite structure. In the accompanying CIFs M1, M2, M3 refer to atom sites Cs14, Cs16|K16|Ow1, and Cs15|K15|Ow3, respectively.

Table 6. Bond Valence Sum Values for Cs at Exchange Site 1

bond	length	S_{ij}
Cs14—O6	3.407(41)	0.072
Cs14—O7	3.789(57)	0.026
Cs14—O7′	3.657(57)	0.037
Cs14—O8	3.405(35)	0.072
Cs14—O9	3.240(34)	0.113
Cs14—O10	3.211(36)	0.122
Cs14—O11	3.845(22)	0.022
Cs14—O11′	3.320(23)	0.091
Cs14—O12	3.375(23)	0.078
Cs14—O12′	3.387(34)	0.076
Cs14—O13	3.499(25)	0.056
Cs14—O13′	3.265(33)	0.105
Cs14—Ow1	3.240(44)	0.113
Cs14—Ow3	3.878(14)	0.020
valence bond sum		1.003

Rietveld refinement for frame 201 (100 min) showed 84% of the Cs^+ located in Exchange Site 1. The NMR spectra of both a 5% and 75% loaded sample, however, show very close resonances at −165 and −172 ppm, respectively. Therefore, even though there is a preference for Exchange Site 1 by Cs^+ cations, the small shift in the NMR spectra at different Cs^+ occupancy levels indicates that the electronic environment of both sites are similar. The presence of the observed spinning side bands is suggested by Norby and co-workers to indicate that the cations are not mobile on the NMR time scale at room temperature.[45]

SUMMARY

The path of Cs^+ as it is incorporated into a H^+-bearing form of potassium zirconium umbite-(HK) was followed in situ by XRD scattering studies. A two-step exchange process of the K^+ cations must occur first for the incoming Cs^+ cations to reach their preferred exchange site in the two unique cavities. This rearrangement leads to extra-framework cation disorder in Exchange Site 2 and is likely the reason for the structural transition. Cations in Exchange Site 2 (positions M2 and M3) do not fit the inversion center when the space group is $P2_1/c$; therefore, the space group cannot stay centrosymmetric. The change in structure is not accompanied by any measurable framework rearrangement as the bond angles and bond distances do not change significantly. The valence bond sum for Cs in Site 1 shows that framework O^{2-} up to 4 Å away from the Cs^+ cation contributes to the bonding.

The ion exchange model proposed herein demonstrates that ion diffusion through many microporous structures can be a multi-step process and not a simple single continuous displacement of ions. In concert with recently published work of in situ time-resolved studies of ion exchange in porous structures[17,46] it is suggested that multi-step ion exchange processes are a fundamental physicochemical properties of these materials. The actual steps and mechanisms may vary from structure to structure just as the ion tunnels in proteins have many mechanisms and steps for cation transfer. Future time-resolved studies of ion exchange will be required to completely characterize and categorize all the sequestration mechanisms in microporous frameworks. Such future work could find applications in waste separation and environmental remediation, optimization of industrial ion exchange processes, and selective metal capture for novel catalysts.

ASSOCIATED CONTENT

Supporting Information. Crystallographic data in CIF format. This material is available free of charge via the Internet at http://pubs.acs.org.

AUTHOR INFORMATION

Corresponding Author

*E-mail: aaron.celestian@wku.edu.

■ ACKNOWLEDGMENT

We acknowledge with thanks the U.S. Department of Energy, Environmental Management Science Program Grant De-FG07-01ER6300 with funds supplied through Westinghouse Savannah River Technology Center, thanks to DOE Basic Energy Sciences Grant DE-FG02-03ER15420, and support from the Advanced Materials Institute at WKU.

■ REFERENCES

(1) Corma, A. *Chem. Rev.* **1997**, *97*, 2373.
(2) Sebastian, V.; Lin, Z.; Rocha, J.; Tellez, C.; Santamaria, J. S.; Coronas, J. *Chem. Commun.* **2005**, 3036.
(3) Clearfield, A. *Chem. Rev.* **1988**, *88*, 125.
(4) Mushtaq, A. *J. Radioanal. Nucl. Chem.* **2004**, *262*, 797.
(5) Mishra, S. P.; Tiwari, D.; Prasad, S. K.; Dubey, R. S.; Mishra, M. *J. Radioanal. Nucl. Chem.* **2006**, *268*, 191.
(6) Al-Attar, L.; Dyer, A.; Paajanen, A.; Harjula, R. *J. Mater. Chem.* **2003**, *13*, 2969.
(7) Behrens, E. A.; Poojary, D. M.; Clearfield, A. *Chem. Mater.* **1998**, *10*, 959.
(8) Clearfield, A. *Solid State Sci.* **2001**, *3*, 103.
(9) Nenoff, T. M.; Miller, J. E.; Thoma, S. G.; Trudell, D. E. *Environ. Sci. Technol.* **1996**, *30*, 3630.
(10) Helfferich, F. *Ion Exchange*; McGraw-Hill Book Company, Inc.: New York, 1962.
(11) Boyd, G. E.; Adamson, A. W.; Myers, L. S. *J. Am. Chem. Soc.* **1947**, *69*, 2836.
(12) Vermeulen, T. *Ind. Eng. Chem.* **1953**, *45*, 1664.
(13) Celestian, A. J.; Parise, J. B.; Goodell, C.; Tripathi, A.; Hanson, J. *Chem. Mater.* **2004**, *16*, 2244.
(14) Celestian, A. J.; Medvedev, D. G.; Tripathi, A.; Parise, J. B.; Clearfield, A. *Nucl. Instrum. Methods Phys., Sect. B* **2005**, *238*, 61.
(15) Ciraolo, M. F.; Hanson, J. C.; Grey, C. P. *Microporous Mesoporous Mater.* **2001**, *49*, 111.
(16) Dalconi, M. C.; Alberti, A.; Cruciani, G. *J. Phys. Chem. B* **2003**, *107*, 12973.
(17) Celestian, A. J.; Kubicki, J. D.; Hanson, J.; Clearfield, A.; Parise, J. B. *J. Am. Chem. Soc.* **2008**, *130*, 11689.
(18) Fogg, A. M.; Dunn, J. S.; O'Hare, D. *Chem. Mater.* **1998**, *10*, 356.
(19) Ragavan, A.; Khan, A.; O'Hare, D. *J. Mater. Chem.* **2006**, *16*, 4155.
(20) Ragavan, A.; Khan, A. I.; O'Hare, D. *J. Mater. Chem.* **2006**, *16*, 602.
(21) Plevert, J.; Sanchez-Smith, R.; Gentz, T. M.; Li, H. L.; Groy, T. L.; Yaghi, O. M.; O'Keeffe, M. *Inorg. Chem.* **2003**, *42*, 5954.
(22) Liu, X. S.; Shang, M. Y.; Thomas, J. K. *Microporous Mater.* **1997**, *10*, 273.
(23) Ferreira, A.; Lin, Z.; Rocha, J.; Morais, C. M.; Lopes, M.; Fernandez, C. *Inorg. Chem.* **2001**, *40*, 3330.
(24) Pertierra, P.; Salvado, M. A.; Garcia-Granda, S.; Bortun, A. I.; Khainakov, S. A.; Garcia, J. R. *Inorg. Chem. Commun.* **2002**, *5*, 824.
(25) Lo, F. R.; Lii, K. H. *J. Solid State Chem.* **2005**, *178*, 1017.
(26) Pertierra, P.; Salvado, M. A.; Garcia-Granda, S.; Khainakov, S. A.; Garcia, J. R. *Thermochim. Acta* **2004**, *423*, 113.
(27) Lin, Z.; Rocha, J.; de Jesus, J. D. P.; Ferreira, A. *J. Mater. Chem.* **2000**, *10*, 1353.
(28) Bortun, A. I.; Bortun, L. N.; Poojary, D. M.; Xiang, O. Y.; Clearfield, A. *Chem. Mater.* **2000**, *12*, 294.
(29) Poojary, D. M.; Bortun, A. I.; Bortun, L. N.; Clearfield, A. *Inorg. Chem.* **1997**, *36*, 3072.
(30) Fewox, C. S.; Kirumakki, S. R.; Clearfield, A. *Chem. Mater.* **2007**, *19*, 384.
(31) Celestian, A. J.; Parise, J. B.; Clearfield, A. In *Springer Handbook of Crystal Growth*; Dhanaraj, G., Byrappa, K., Prasad, V., Dudley, M., Eds.; Springer: New York, 2010; p 1637.
(32) Celestian, A. J.; Kubicki, J. D.; Hanson, J.; Clearfield, A.; Parise, J. B. *J. Am. Chem. Soc.* **2008**, *130*, 11689.
(33) Hammersley, A. P. *FIT2D: V9.129 Reference Manual V3.1*; ESRF: Grenoble, 1998.
(34) Hammersley, A. P.; Svensson, S. O.; Hanfland, M.; Finch, A. N.; Hausermann, D. *High Pressure Res.* **1996**, *14*, 235.
(35) Hammersley, A. P.; Svensson, S. O.; Thompson, A. *Nucl. Instrum. Methods Phys. Res., Sect. A* **1994**, *346*, 312.
(36) Hammersley, A. P.; Svensson, S. O.; Thompson, A.; Graafsma, H.; Kvick, A.; Moy, J. P. *Rev. Sci. Instrum.* **1995**, *66*, 2729.
(37) Roisnel, T.; Rodriguez-Carvajal, J. *EPDIC 7, Proc. Eur. Powder Diff.* **2001**, *378-3*, 118; Parts 1 and 2.
(38) Larson, A. C.; VonDreele, R. B. *General Structure Analysis System (GSAS)*. Los Alamos National Laboratory: Los Alamos, NM, 2000.
(39) Le Bail, A.; Duroy, H.; Fourquet, J. L. *Mater. Res. Bull.* **1998**, *23*, 447.
(40) Rietveld, H. M. *J. Appl. Crystallogr.* **1969**, *2*, 65.
(41) Toby, B. H. *J. Appl. Crystallogr.* **2001**, *34*, 210.
(42) Fewox, C. S.; Clearfield, A. *J. Phys. Chem. A* **2008**, *112*, 2589.
(43) Brown, I. D.; Altermatt, D. *Acta Crystallogr., Sect. B* **1985**, *41*, 244.
(44) Wills, A. S. *VaList*, 4.0.6 ed.; 2010.
(45) Norby, P.; Poshni, F. I.; Gualtieri, A. F.; Hanson, J. C.; Grey, C. P. *J. Phys. Chem. B* **1998**, *102*, 839.
(46) Lopano, C. L.; Heaney, P. J.; Post, J. E. *Am. Mineral.* **2009**, *94*, 816.